EUROPEAN ORGANIZATION FOR NUCLEAR RESEARCH

CERN–EP – 2000–141
November 2, 2000

Transverse momentum distributions of J/ψ, ψ', Drell-Yan and continuum dimuons produced in Pb-Pb interactions at the SPS

NA50 Collaboration

M.C. Abreu[7,a)], B. Alessandro[11)], C. Alexa[4)], R. Arnaldi[11)], M. Atayan[13)], C. Baglin[2)], A. Baldit[3)], M. Bedjidian[12)], F. Bellaiche[12)], S. Beolè[11)], V. Boldea[4)], P. Bordalo[7,b)], A. Bussière[2)], L. Capelli[12)], V. Capony[2)], L. Casagrande[7,c)], J. Castor[3)], T. Chambon[3)], B. Chaurand[10)], I. Chevrot[3)], B. Cheynis[12)], E. Chiavassa[11)], C. Cicalò[5)], M.P. Comets[9)], N. Constans[10)], S. Constantinescu[4)], J. Cruz[7)], A. De Falco[5)], G. Dellacasa[1)], N. De Marco[11)], A. Devaux[3)], S. Dita[4)], O. Drapier[12)], L. Ducroux[12)], B. Espagnon[3)], J. Fargeix[3)], P. Force[3)], M. Gallio[11)], Y.K. Gavrilov[8)], C. Gerschel[9)], P. Giubellino[11)], M.B. Golubeva[8)], M. Gonin[10)], A.A. Grigorian[13)], J.Y. Grossiord[12)], F.F. Guber[8)], A. Guichard[12)], H. Gulkanyan[13)], R. Hakobyan[13)], R. Haroutunian[12)], M. Idzik[11,d)], D. Jouan[9)], T.L. Karavitcheva[8)], L. Kluberg[10)], A.B. Kurepin[8)], Y. Le Bornec[9)], C. Lourenço[6)], M. Mac Cormick[9)], P. Macciotta[5)], A. Marzari-Chiesa[11)], M. Masera[11)], A. Masoni[5)], S. Mehrabyan[13)], M. Monteno[11)], S. Mourgues[3)], A. Musso[11)], F. Ohlson-Malek[12,e)], P. Petiau[10)], A. Piccotti[11)], J.R. Pizzi[12)], F. Prino[11)], G. Puddu[5)], C. Quintans[7)], L. Ramello[1)], S. Ramos[7,b)], P. Rato-Mendes[7)], L. Riccati[11)], A. Romana[10)], I. Ropotar[6,f)], P. Saturnini[3)], E. Scomparin[11)], S. Serci[5)], R. Shahoyan[7,g)], S. Silva[7)], M. Sitta[1)], C. Soave[11)], P. Sonderegger[6,b)], X. Tarrago[9)], N.S. Topilskaya[8)], G.L. Usai[5)], E. Vercellin[11)], L. Villatte[9)], N. Willis[9)]

Abstract

Muon pairs produced in Pb-Pb interactions at 158 GeV/c per nucleon are used to study the transverse momentum distributions of the J/ψ, ψ' and dimuons in the mass continuum. In particular, the dependence of these distributions on the centrality of the Pb-Pb collision is investigated in detail.

Submitted to Phys. Lett. B

[1)] Università del Piemonte Orientale, Alessandria and INFN-Torino, Italy
[2)] Laboratoire de Physique des Particules (LAPP), IN2P3-CNRS, Annecy-le-Vieux, France
[3)] Laboratoire de Physique Corpusculaire (LPC), Université Blaise Pascal, IN2P3-CNRS, Aubière, France
[4)] Institute of Atomic Physics (IFA), Bucharest, Romania
[5)] Università di Cagliari / INFN, Cagliari, Italy
[6)] CERN, Geneva, Switzerland
[7)] Laboratório de Instrumentação e Física de Partículas (LIP), Lisbon, Portugal
[8)] Institute for Nuclear Research (INR), Moscow, Russia
[9)] Institut de Physique Nucléaire de Orsay (IPNO), Université Paris-Sud, IN2P3-CNRS, Orsay, France
[10)] Laboratoire de Physique Nucléaire des Hautes Energies (LPNHE), Ecole Polytechnique, IN2P3-CNRS, Palaiseau, France
[11)] Università di Torino / INFN, Torino, Italy
[12)] Institut de Physique Nucléaire de Lyon (IPNL), Université Claude Bernard, IN2P3-CNRS, Villeurbanne, France
[13)] Yerevan Physics Institute (YerPhI), Yerevan, Armenia
[a)] Also at UCEH, Universidade do Algarve, Faro, Portugal
[b)] Also at IST, Universidade Técnica de Lisboa, Lisbon, Portugal
[c)] Now at CERN, Geneva, Switzerland
[d)] Now at FPNT, University of Mining and Metallurgy, Cracow, Poland
[e)] Now at ISN, Univ. Joseph Fourier and IN2P3-CNRS, Grenoble, France
[f)] Also at University of Wuppertal, Wuppertal, Germany
[g)] On leave of absence from YerPhI, Yerevan, Armenia

1 Introduction

Among the signals suggested to identify the existence of a phase transition to a quark-gluon plasma (QGP) in ultrarelativistic heavy-ion collisions, the suppression of J/ψ production, as proposed by T. Matsui and H. Satz [1], is considered as the most directly related to deconfinement. The NA38 collaboration has observed that the J/ψ production is suppressed in collisions of oxygen and sulphur ions with a uranium target [2, 3]. However, these results can be explained by a normal absorption mechanism in nuclear matter [4]. More recently, the NA50 collaboration has measured the J/ψ production in Pb-Pb collisions at 158 GeV/c per nucleon [5, 6, 7]. For peripheral Pb-Pb collisions, the yield of J/ψ agrees with the results obtained in proton and light ion induced reactions. For the most central Pb-Pb collisions, it is found to be significantly lower than the value extrapolated from the measurements made on lighter systems and taken as a baseline. This discontinuous behaviour shows the presence of a physical threshold for the measured yield and can be well explained if a quark-gluon plasma is formed in the collision [8, 9].

Several alternative mechanisms have been proposed to account for these results, such as destructive interactions with hadronic comovers [10, 11] or with prompt gluons [12]. None of them can accomodate the kind of threshold visible in the data. Furthermore, the most recent experimental results [13] show a steady decrease in the J/ψ production rate for the most central collisions; they rule out the models based on these alternative mechanisms, which are all unable to account for the suppression rate observed for the most central Pb-Pb collisions. The study of the J/ψ transverse momentum distribution could provide additional interesting information and a deeper insight into the underlying physical process.

Preliminary results on the p_{T} distribution of J/ψ mesons produced in Pb-Pb collisions have already been reported [14, 15]. This paper presents the final analysis of p_{T} distributions of J/ψ, ψ', Drell-Yan (DY) and muon pairs in the mass continuum between 2.1 and 2.7 GeV/c^2 (the intermediate mass region or IMR). The analysis uses the high statistics data sample of Pb-Pb collisions collected at the CERN SPS in 1996.

2 Experimental set-up and data samples

The NA50 experiment makes use basically of a muon spectrometer to measure the production of muon pairs as a function of the centrality of the collision. The main characteristics of the set-up are given hereafter. A more detailed description of the layout can be found in Ref. [5].

Dimuons are detected in the kinematical domain defined by $0 \leq y_{cm} \leq 1$ and $-0.5 \leq \cos\theta_{CS} \leq 0.5$, where y_{cm} is the dimuon rapidity in the center of mass frame and θ_{CS} is the polar decay angle of the muons in the Collins-Soper frame [16].

Three detectors can provide an estimate of the centrality of the collision: an electromagnetic calorimeter which measures the neutral transverse energy (E_{T}) produced in the pseudo-rapidity interval $1.1 \leq \eta_{\mathrm{lab}} \leq 2.3$; a zero degree hadronic calorime-

ter which measures the energy of the beam fragments ($E_{\rm ZDC}$) at $\eta_{\rm lab} > 6.3$; and a multiplicity detector which measures the charged particle multiplicity in the range $1.65 \leq \eta_{\rm lab} \leq 3.5$. In what follows, the centrality of the collision is estimated from the neutral transverse energy following a procedure described in Ref. [5].

The yield of events is maximized thanks to an active target made of seven Pb subtargets spaced 25 mm apart. The target device is instrumented with quartz blades, two blades per subtarget, located off the beam axis [17], which are used to identify the precise vertex of the interaction. A total target thickness of 12 mm (7 mm) corresponding to 30 % (17 %) of an interaction length has been used for the 1996 (1995) data taking periods. Finally, a beam hodoscope counts the incident ions and different anti-halo detectors allow the rejection of events for which a primary interaction occurred upstream of the target.

The identification of the vertex of the interaction, as originally requested in the analysis of the data collected in 1995 [5], induces a significant loss in the number of peripheral reactions left in the final sample of events. The loss is due to the low efficiency of the identification procedure when the number of secondaries produced in the interaction is small (the blades of the active target only cover a small fraction of the solid angle). In the data sample analyzed in this paper, the selection of on-target events is extended and based on the $E_{\rm T} - E_{\rm ZDC}$ correlation, as detailed in Ref. [7]. On-target events are selected within a contour of 2σ width around the mean correlation. For events satisfying this selection, if the subtarget where the interaction has occured is not directly identified (and only in this case), the event is treated as if it had been produced in the central subtarget. The statistics of the low $E_{\rm T}$ sample is thus substantially increased. The on-target feature of the additional events is verified using empty target measurements. The new selection method is made possible thanks to the excellent 1996 beam conditions and to the different anti-halo detectors. Other details on data taking conditions and event selection can been found in Refs. [5, 7]. The final event samples contain $170 \cdot 10^6$ triggers and $\sim 190\,000$ J/ψ events in 1996, and $60 \cdot 10^6$ triggers and $\sim 50\,000$ J/ψ events in 1995.

3 Analysis

For masses higher than 1.5 GeV/c^2, the contributions to the invariant mass distribution of opposite-sign muon pairs originate from four known sources: the Drell-Yan process (DY), the J/ψ and ψ' decays and the semi-leptonic decay of pairs of charmed mesons ($D\bar{D}$). The spectrum includes also the contribution of a combinatorial background originating from uncorrelated π and K decays. This background is estimated from the samples of like-sign muon pairs. The opposite-sign muon pair mass spectrum of the selected data sample is shown in Fig. 1.

The study of the physical $p_{\rm T}$ distributions of the IMR, J/ψ, ψ' and DY dimuons requires a correction for the detector acceptance and smearing, which may depend on the other kinematical variables M, y_{cm} and $\cos\theta_{CS}$. In the mass regions where there

is essentially one dominant known process (J/ψ, ψ', DY) these other distributions can be chosen so as to reproduce the experimental ones, and the one-dimensional (1-D) $p_{\rm T}$ acceptance of each process can thus be computed using the NA50 Monte-Carlo generation and reconstruction codes. In this case, generated events are tracked through the apparatus and reconstructed using the same procedure as applied to the experimental data. This 1-D acceptance calculation does not hold when a physical process of unknown character is present in the measured spectrum as is the case for the intermediate mass region where, on top of Drell-Yan and $D\bar{D}$ muon pairs, other unknown processes could contribute [18]. In this case, the problem has to be solved with a four-dimensional (4-D) method. The algorithm developed for this study is based on an image restoration technique, which has been extended to four dimensions. It does not require any a priori hypothesis on the shapes of the distributions of the kinematical variables of the different processes involved. Moreover, possible physical correlations among the different variables are preserved in the method. Details on this deconvolution procedure can be found in Ref. [19], together with the corresponding background subtraction technique.

Therefore, two different methods have been used to correct the measured kinematical distributions for detector effects: the 4-D unfolding procedure has been applied for events in the IMR mass range ($2.1 < M < 2.7$ GeV/c^2), and the simpler 1-D acceptance and smearing correction method has been applied to the J/ψ, ψ' and DY mass regions. In order to take into account the contribution of the mass continuum events under the resonance peaks, the invariant mass spectrum, after background subtraction, is fitted to the sum of the four contributions: J/ψ, ψ', DY and $D\bar{D}$. For $M > 4.2$ GeV/c^2, only DY contributes. In the J/ψ region, the continuum contribution amounts to less than 8 % of the total in the mass range $2.7 < M < 3.5$ GeV/c^2, and to 3 % in the narrower interval ($2.9 < M < 3.3$ GeV/c^2) which contains about 90 % of the J/ψ's. These continuum events are mainly DY pairs. This leads us to consider different ways of correcting the $p_{\rm T}$ distributions for the contribution of the mass continuum events. For the wider J/ψ mass range, two $p_{\rm T}$ distributions are used, corresponding to the experimental IMR and DY ones. For the narrower J/ψ mass range, the $p_{\rm T}$ distribution of DY extrapolated from the high mass interval to the mass region under consideration is subtracted. For the 1995 data, only the wider J/ψ mass range and the DY $p_{\rm T}$ distributions for the continuum events were used.

In the case of the ψ' ($3.5 < M < 3.9$ GeV/c^2), the correction is done using either the experimental $p_{\rm T}$ distribution of DY events, or a superposition of J/ψ, DY and $D\bar{D}$ Monte-Carlo contributions, the yields of which are deduced from the mass fit. The results obtained with the different corrections are compatible within errors. As the continuum contribution amounts to 50 % in the ψ' mass range, the 4-D deconvolution method has also been applied and leads to a result compatible with the 1-D correction.

4 Transverse momentum distributions

Figure 2 shows the $p_{\rm T}$ distributions, integrated over the impact parameter, for different invariant mass ranges. In order to investigate the centrality dependence, the events are divided into subsamples according to the transverse energy produced in the collision. For J/ψ and IMR events, the size of the samples allows 15 centrality bins while for ψ' and DY events, as well as for the J/ψ events collected in 1995, the number of bins is limited to 5. The $\langle p_{\rm T} \rangle$ and $\langle p_{\rm T}^2 \rangle$ values obtained for the different mass intervals are shown in Tables 1, 2 and 3, and plotted in Figs. 3 and 4 as a function of $E_{\rm T}$. The subtraction of the contribution of the mass continuum below the J/ψ induces a systematic uncertainty on the $\langle p_{\rm T}^2 \rangle$ values of the J/ψ of 2 %. The $\langle p_{\rm T}^2 \rangle$ values for the J/ψ obtained from the 1995 data sample are also plotted in Fig. 4. For the J/ψ, the values of $\langle p_{\rm T} \rangle$ and $\langle p_{\rm T}^2 \rangle$ first increase and then tend to flatten when the centrality of the collision increases. The $\langle p_{\rm T}^2 \rangle$ values obtained from the 1995 and 1996 data are in good agreement all over the measured transverse energy range, despite the different target thicknesses. This suggests that no significant bias due to undetected reinteractions affects this quantity. The $\langle p_{\rm T}^2 \rangle$ values for the ψ' are higher than those of the J/ψ.

The $\langle p_{\rm T}^2 \rangle$ values of J/ψ produced in collisions induced by lighter projectiles (p, O, S) [20, 21, 22] have been successfully interpreted in terms of initial-state parton multiple scattering [23, 24]. Since the amount of matter traversed by the produced J/ψ tends to saturate with $E_{\rm T}$ in a symmetric system like Pb-Pb, because of collision geometry, the $\langle p_{\rm T} \rangle$ and $\langle p_{\rm T}^2 \rangle$ values are expected to saturate at high $E_{\rm T}$, as observed. The dependence of $\langle p_{\rm T}^2 \rangle$ with centrality in Pb-Pb collisions, based on initial state interactions, has been calculated in Refs. [25, 26]. However, none of these calculations can be directly compared to the results reported in this paper, since they do not take into account the fact that the $\langle p_{\rm T}^2 \rangle$ value in pp collisions depends on the beam energy, as observed for the first time by the NA3 experiment with pion beams [20]. A difference is indeed expected between 200 and 158 GeV/nucleon and the parameters deduced from the 200 GeV measurements in p-A and S-U collisions cannot be directly applied to 158 GeV. The overall trend of the $\langle p_{\rm T}^2 \rangle$ pattern, however, is not affected by this problem. In Ref. [27] the formation of a QGP is expected to induce a change in the J/ψ transverse momentum distributions, increasing $\langle p_{\rm T}^2 \rangle$, since high-$p_{\rm T}$ J/ψ's can escape without being suppressed by the plasma. Ref. [26] takes into account the fact that the $p_{\rm T}$ value can only be measured for those J/ψ's which are not absorbed. This leads to a reduction in the effective amount of matter traversed by the detected J/ψ mesons. In fact, if the absorption is strong enough for central Pb-Pb collisions, as in the case of QGP formation, the $\langle p_{\rm T}^2 \rangle$ value could even decrease at high $E_{\rm T}$. Such effects are not seen in the data.

In order to study more precisely the effect of initial state interactions, the $\langle p_{\rm T}^2 \rangle$ values are plotted as a function of the length of matter crossed by the produced J/ψ meson, L, a quantity directly related to the number of nucleons involved in these interactions. Figure 5 includes the different measurements made at 200 GeV/nucleon [20,

21, 22] together with the Pb-Pb data. The results are fitted according to the formalism of Ref. [24], $\langle p_{\rm T}^2\rangle(E_{\rm T}) = \langle p_{\rm T}^2\rangle_{pp} + a_{gN}\ L(E_{\rm T})$, where $\langle p_{\rm T}^2\rangle(E_{\rm T})$ and $L(E_{\rm T})$ are, respectively, the $\langle p_{\rm T}^2\rangle$ and L values in a given $E_{\rm T}$ bin. The results of the fit are shown in Table 4 and in Fig. 5. The slopes are compatible and the difference in the $\langle p_{\rm T}^2\rangle_{pp}$ values between the two beam energies is of the order of 0.10 $({\rm GeV}/c)^2$. The result of a simultaneous fit to the 200 GeV and Pb-Pb data with a common slope is also shown in Table 4.

In order to study the J/ψ suppression as a function of the transverse momentum, we have calculated the ratios $R_i(p_{\rm T})$ between the $p_{\rm T}$ distributions obtained in the $E_{\rm T}$ bin i and the same distribution obtained in the first $E_{\rm T}$ bin. They are normalized to the number of muon pairs with mass $M > 4.2$ GeV/c^2 in the same $E_{\rm T}$ bins. These ratios are plotted in Fig. 6 for the centrality bins of Table 3. The suppression is clearly stronger at low $p_{\rm T}$. Due to the small number of events above $p_{\rm T}$ around 3 GeV/c, it is not possible to clarify if these ratios saturate or continue to grow at high $p_{\rm T}$, a question addressed in Ref. [27].

5 Transverse mass distributions

The transverse mass distributions of the produced muon pairs have also been studied in order to allow a comparison with thermal models [28]. The $(M_{\rm T}-M)$ distributions, where $M_{\rm T} = \sqrt{p_{\rm T}^2 + M^2}$, are calculated from the experimental data in the different mass regions and are plotted in Fig. 7. The $M_{\rm T}$ distribution of the J/ψ is fitted, for each of the 15 transverse energy bins, with the analytical function, $1/T \cdot M_{\rm T}^2 \cdot K_1(M_{\rm T}/T)$, where K_1 is the modified Bessel function and the inverse slope T is related to the temperature of the system in thermal models. The $\langle M_{\rm T} - M\rangle$ and T values for the J/ψ are shown in Table 5. The inverse slope T is also plotted in Fig. 8 as a function of the transverse energy, $E_{\rm T}$. Both variables have a similar behaviour. They first increase with $E_{\rm T}$ and then seem to flatten at high $E_{\rm T}$, as the $\langle p_{\rm T}\rangle$ and $\langle p_{\rm T}^2\rangle$ values. The $M_{\rm T}$ spectra have also been fitted with the exponential function $M_{\rm T} \cdot \exp\left(-(M_{\rm T} - M)/T\right)$. The general behaviour of T versus $E_{\rm T}$ is similar to the one obtained with the modified Bessel function but the absolute values are 5 to 10 MeV higher.

Conclusions

The transverse momentum distributions of muon pairs produced in Pb-Pb collisions at 158 GeV per nucleon have been studied as a function of the centrality of the collisions. The $\langle p_{\rm T}\rangle$ and $\langle p_{\rm T}^2\rangle$ values have been determined for muon pairs of different origins: intermediate mass region (IMR), the J/ψ and ψ' decays, and the Drell-Yan mechanism. The $\langle p_{\rm T}^2\rangle$ values for the ψ' are higher than for the J/ψ. For the J/ψ, the values $\langle p_{\rm T}\rangle$, $\langle p_{\rm T}^2\rangle$, $\langle M_{\rm T} - M\rangle$ and the inverse slope parameter, T, exhibit a similar trend as a function of $E_{\rm T}$: an initial increase followed by a flatter behaviour. The

comparison of the 1995 and 1996 results suggests that the $\langle p_{\rm T}^2 \rangle$ values of the J/ψ, for the most central events, are not affected by re-interaction effects due to the thickness of the target.

The change of the $p_{\rm T}$ distributions with the centrality of the collision agrees with what is expected from interactions in the initial state. The present statistics does not allow a precise study of the high $p_{\rm T}$ behaviour.

This work was partially supported by Fundação para a Ciência e a Tecnologia, by INTAS grant 96-0231 and by the Russian Foundation for Fundamental Research, grant 99-02-16003.

References

[1] T. Matsui and H. Satz, Phys. Lett. B 178 (1986) 416.
[2] NA38 Collaboration, C. Baglin et al., Phys. Lett. B 255 (1991) 459;
NA38 Collaboration, C. Baglin et al., Phys. Lett. B 345 (1995) 617.
[3] NA38 Collaboration, C. Baglin et al., Phys. Lett. B 466 (1999) 408.
[4] C. Gerschel and J. Hüfner, Z.Phys. C 56 (1992) 71.
[5] NA50 Collaboration, M.C. Abreu et al., Phys. Lett. B 410 (1997) 327.
[6] NA50 Collaboration, M.C. Abreu et al., Phys. Lett. B 410 (1997) 337.
[7] NA50 Collaboration, M.C. Abreu et al., Phys. Lett. B450 (1999) 456.
[8] J.P. Blaizot and J.Y. Ollitrault, Phys. Rev. Lett. 77 (1996) 1703;
C.Y. Wong, Phys. Rev. C 55 (1997) 2621.
[9] D. Kharzeev et al., Z. Phys. C 74 (1997) 307.
[10] A. Capella et al., Phys. Lett. B 393 (1997) 431.
[11] S. Gavin and R. Vogt, Phys. Rev. Lett. 78 (1997) 1006.
[12] J. Hüfner and B.Z. Kopeliovich, Phys. Lett. B 445 (1998) 223;
J. Hüfner et al., Eur. Phys. J. A7 (2000) 239.
[13] NA50 Collaboration, M.C. Abreu et al., Phys. Lett. B 477 (2000) 28.
[14] NA50 Collaboration, M.C. Abreu et al., Nucl. Phys. A 638 (1998) 261c.
[15] NA50 Collaboration, M.C. Abreu et at., Nucl. Phys. A 654 (1999) 640c.
[16] J.L. Collins and D.E. Soper, Phys. Rev. D 16 (1977) 2219.
[17] F. Bellaiche et al., Nucl. Inst. Meth. A 398 (1997) 180.
[18] NA50 Collaboration, M.C. Abreu et al., Jour. Phys. G 25 (1999) 235,
NA50 Collaboration, M.C. Abreu et al., Eur. Phys. J. C 14 (2000) 443.
[19] NA38 Collaboration, M.C. Abreu et al., Nucl. Inst. Meth. A 405 (1998) 139.
[20] NA3 Collaboration, J. Badier et al., Z. Phys. C 20 (1983) 101.
[21] NA38 Collaboration, C. Baglin et al., Phys. Lett. B 262 (1991) 362.
[22] NA38 Collaboration, M.C. Abreu et al., Phys. Lett. B 423 (1998) 207.
[23] S. Gavin and M. Gyulassy, Phys. Lett. B 214 (1988) 241;
J.P. Blaizot and J.Y. Ollitrault, Phys. Lett. B 217 (1989) 392.
[24] J. Hüfner, Y. Kurihara and H.J. Pirner, Phys. Lett. B 215 (1988) 218.
[25] S. Gavin and R. Vogt, hep-ph/9610432.

[26] D. Kharzeev, M. Nardi and H. Satz, Phys. Lett. B 405 (1997) 14.
[27] K. Karsch and R. Petronzio, Phys. Lett. B 193 (1987) 105;
M.C. Chu and T. Matsui, Phys. Rev. D 37 (1988) 1851;
J.P. Blaizot and J.Y. Ollitrault, Phys. Rev. D 39 (1989) 232.
[28] R. Hagedorn, Riv. Nuovo Cimento 6 (1983) 1.

Table 1: Mean values of $p_{\rm T}$ and $p_{\rm T}^2$ calculated from the IMR distributions in 15 $E_{\rm T}$ bins. The average $E_{\rm T}$ value in each bin is also given.

$E_{\rm T}$ range	$\langle E_{\rm T}\rangle$	$2.1 < M < 2.7$ (GeV/c^2)	
(GeV)	(GeV)	$\langle p_{\rm T}\rangle$ (GeV/c)	$\langle p_{\rm T}^2\rangle$(GeV/$c$)^2
5-20	14	0.810 ± 0.017	0.872 ± 0.039
20-27	24	0.854 ± 0.022	0.994 ± 0.051
27-34	32	0.915 ± 0.021	1.138 ± 0.053
34-43	41	0.862 ± 0.020	1.041 ± 0.049
43-51	49	0.879 ± 0.021	1.069 ± 0.053
51-60	56	0.811 ± 0.019	0.944 ± 0.047
60-66	63	0.877 ± 0.022	1.032 ± 0.054
66-74	70	0.883 ± 0.021	1.096 ± 0.054
74-80	77	0.903 ± 0.023	1.110 ± 0.058
80-86	83	0.880 ± 0.025	1.089 ± 0.066
86-93	90	0.920 ± 0.022	1.163 ± 0.056
93-100	97	0.916 ± 0.024	1.130 ± 0.061
100-107	103	0.860 ± 0.025	1.032 ± 0.061
107-114	110	0.927 ± 0.030	1.198 ± 0.078
114-140	119	0.924 ± 0.037	1.174 ± 0.093

Table 2: Mean values of $p_{\rm T}$ and $p_{\rm T}^2$ calculated from the J/ψ distributions in 15 $E_{\rm T}$ bins. The calculated value of L in each $E_{\rm T}$ bin is also given.

$E_{\rm T}$ range (GeV)	L (fm)	J/ψ	
		$\langle p_{\rm T}\rangle$ (GeV/c)	$\langle p_{\rm T}^2\rangle$ (GeV/c)^2
5-20	4.9 ± 0.7	1.072 ± 0.005	1.504 ± 0.012
20-27	6.2 ± 0.4	1.108 ± 0.007	1.603 ± 0.021
27-34	7.0 ± 0.3	1.130 ± 0.006	1.670 ± 0.019
34-43	7.5 ± 0.3	1.136 ± 0.007	1.691 ± 0.020
43-51	7.9 ± 0.2	1.151 ± 0.007	1.735 ± 0.021
51-60	8.2 ± 0.2	1.176 ± 0.008	1.799 ± 0.023
60-66	8.4 ± 0.2	1.174 ± 0.006	1.804 ± 0.020
66-74	8.7 ± 0.2	1.176 ± 0.009	1.825 ± 0.027
74-80	8.9 ± 0.2	1.179 ± 0.007	1.831 ± 0.022
80-86	9.1 ± 0.2	1.192 ± 0.009	1.853 ± 0.025
86-93	9.2 ± 0.2	1.183 ± 0.007	1.844 ± 0.022
93-100	9.4 ± 0.1	1.187 ± 0.010	1.827 ± 0.030
100-107	9.5 ± 0.1	1.191 ± 0.009	1.864 ± 0.028
107-114	9.6 ± 0.1	1.196 ± 0.012	1.870 ± 0.035
114-140	9.7 ± 0.1	1.222 ± 0.014	1.946 ± 0.043

Table 3: Mean values of $p_{\rm T}$ and $p_{\rm T}^2$ calculated from the ψ' and Drell-Yan distributions for 5 $E_{\rm T}$ bins.

$E_{\rm T}$ range (GeV)	$\langle E_{\rm T}\rangle$ (GeV)	ψ'		DY ($M > 4.2$ GeV/c^2)	
		$\langle p_{\rm T}\rangle$(GeV/c)	$\langle p_{\rm T}^2\rangle$ (GeV/c)^2	$\langle p_{\rm T}\rangle$(GeV/c)	$\langle p_{\rm T}^2\rangle$ (GeV/c)^2
5-34	23	1.11 ± 0.05	1.64 ± 0.13	0.94 ± 0.03	1.16 ± 0.09
34-60	48	1.20 ± 0.08	1.97 ± 0.25	1.06 ± 0.03	1.51 ± 0.09
60-80	70	1.33 ± 0.10	2.24 ± 0.31	1.01 ± 0.03	1.46 ± 0.08
80-100	90	1.40 ± 0.16	2.66 ± 0.54	1.06 ± 0.04	1.52 ± 0.11
100-140	110	1.45 ± 0.20	2.54 ± 0.56	1.06 ± 0.05	1.57 ± 0.14

Table 4: Parameters of the linear fits to the L-dependence of the J/ψ $\langle p_{\rm T}^2 \rangle$. See Fig. 5. The last line corresponds to the simultaneous fit to both data sets.

Beam energy (GeV)	$\langle p_{\rm T}^2 \rangle_{pp}$ ((GeV/c)^2)	a_{gN} ((GeV/c)^{2}fm^{-1})	χ^2/ndf
200	1.21±0.03	0.078±0.006	0.8
158	1.11±0.03	0.081±0.004	0.6
200	1.20±0.02	0.080±0.003	0.65
158	1.11±0.02		

Table 5: Mean values of $M_{\rm T} - M$ calculated from the J/ψ distributions for the 15 $E_{\rm T}$ bins. The parameter T and the value χ^2/ndf are obtained from a fit with the modified Bessel function.

$\langle E_{\rm T} \rangle$ (GeV)	$\langle M_{\rm T} - M \rangle$ (MeV/c^2)	T (MeV)	χ^2/ndf
14	226 ± 2	207 ± 2	1.1
24	239 ± 3	217 ± 2	1.1
32	249 ± 2	224 ± 2	1.3
41	252 ± 3	230 ± 2	0.6
49	258 ± 2	233 ± 2	1.8
56	267 ± 3	240 ± 2	1.1
63	267 ± 3	240 ± 2	1.2
70	269 ± 4	241 ± 2	1.1
77	271 ± 3	242 ± 2	1.9
83	273 ± 5	244 ± 3	0.7
90	272 ± 3	245 ± 3	0.8
97	273 ± 5	245 ± 3	1.3
103	274 ± 4	245 ± 3	1.1
110	275 ± 5	248 ± 3	1.3
119	284 ± 6	255 ± 4	1.8

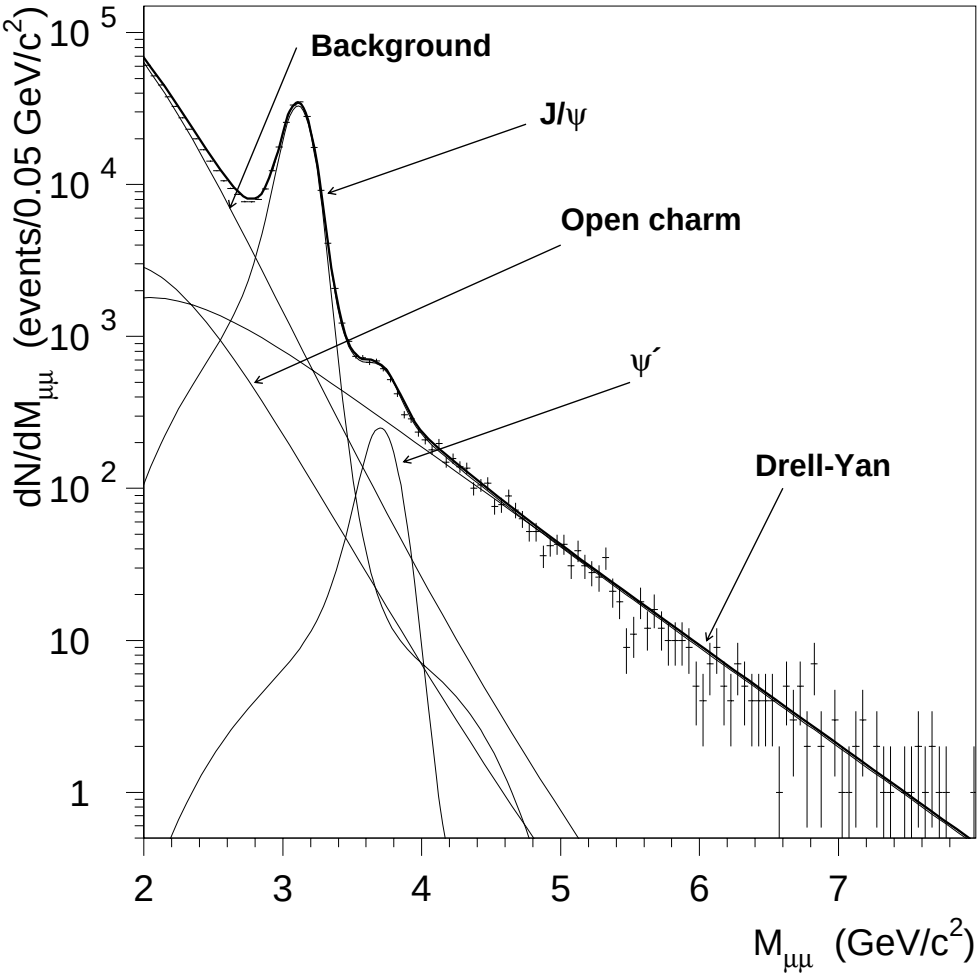

Figure 1: Opposite-sign muon pair invariant mass spectrum for Pb-Pb collisions at 158 GeV/c incident momentum. Data collected in 1996.

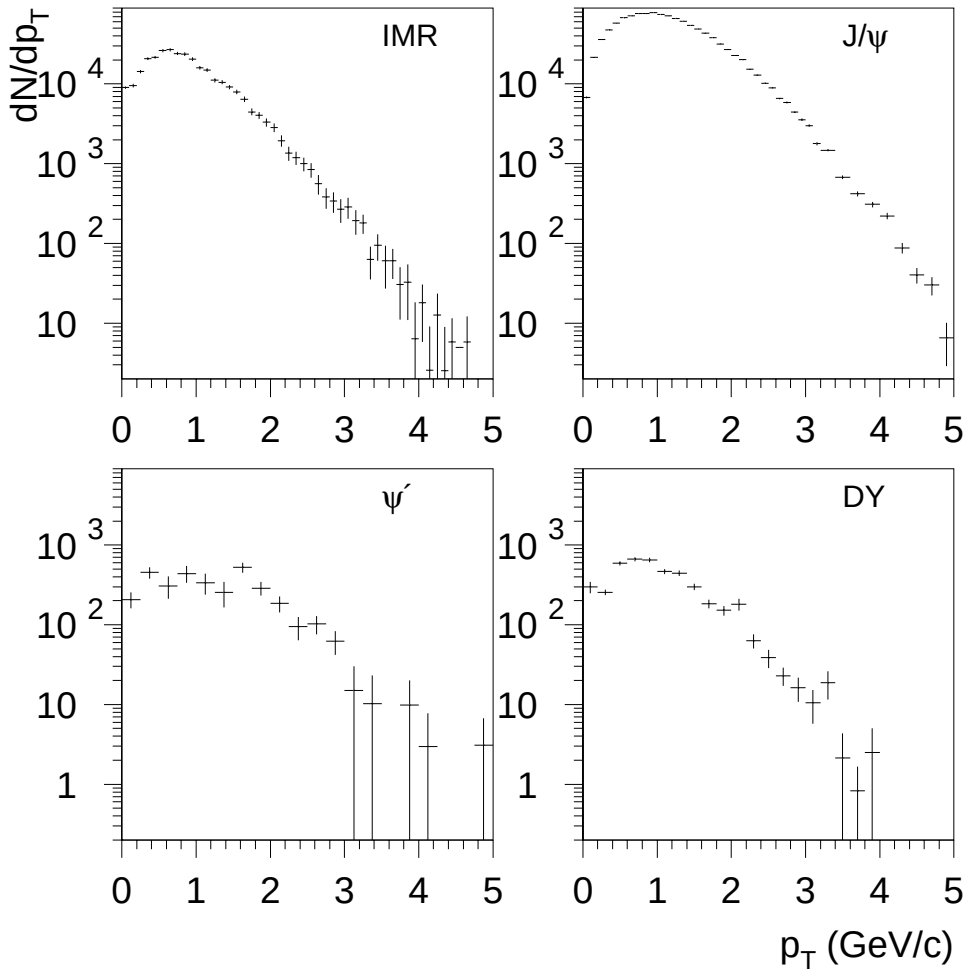

Figure 2: p_{T} distributions for several muon pair mass intervals. IMR stands for the mass range $2.1 < M < 2.7$ GeV/c^2 and DY stands for $M > 4.2$ GeV/c^2.

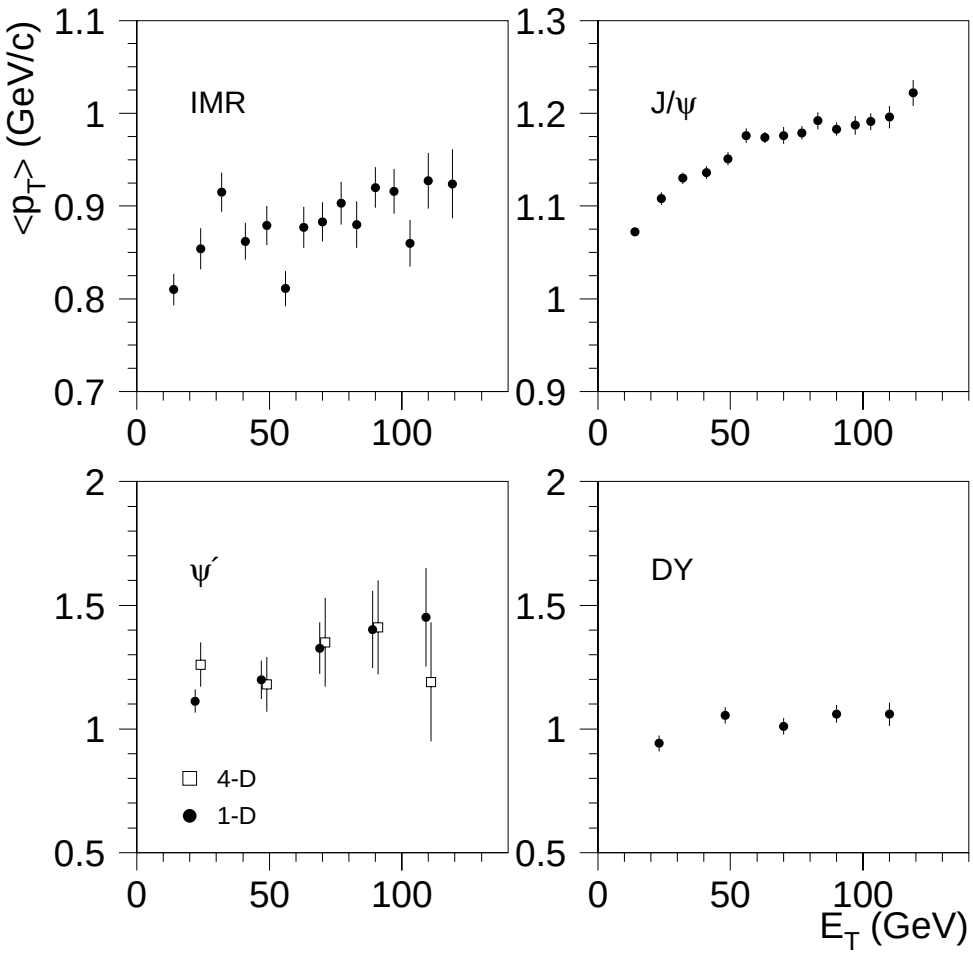

Figure 3: $\langle p_{\rm T} \rangle$ as a function of the transverse energy for several muon pair mass intervals. The error bars are only statistical. For the ψ', both the 1-D and 4-D deconvolution results are shown.

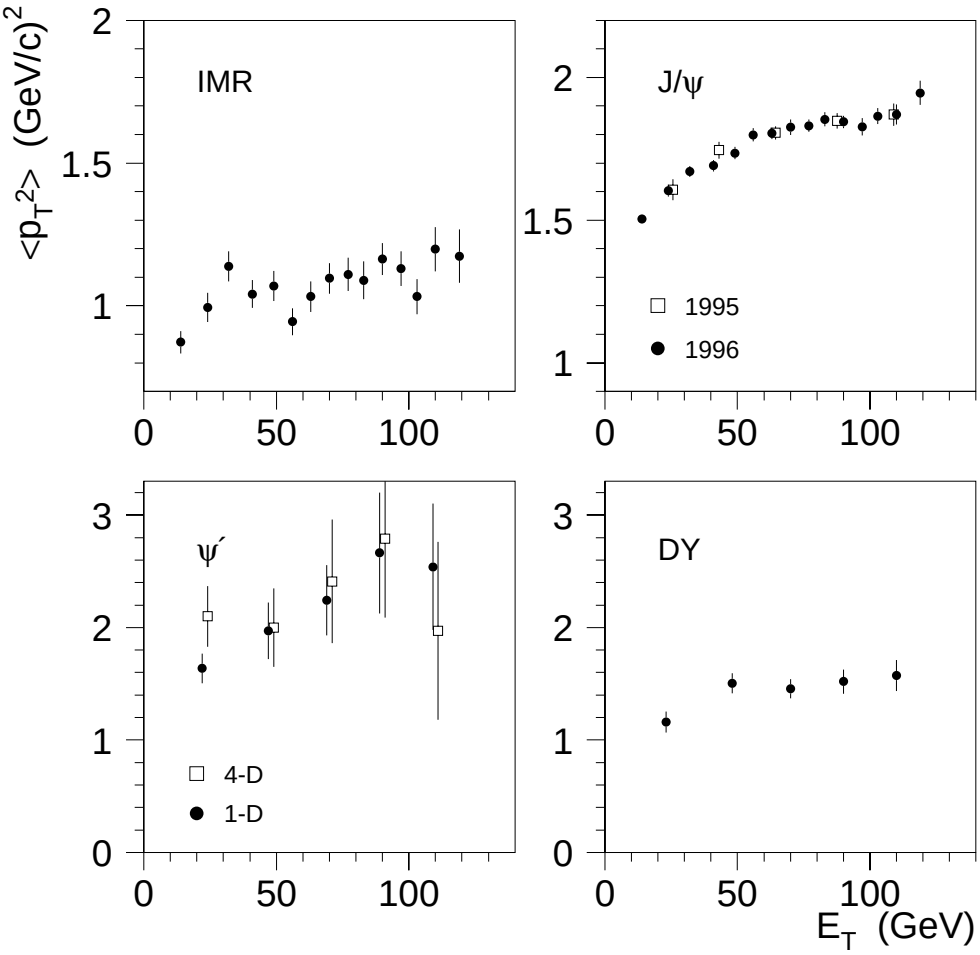

Figure 4: $\langle p_{\mathrm{T}}^2 \rangle$ as a function of the transverse energy for several muon pair mass intervals. For the J/ψ, the 5 open squares correspond to the 1995 data sample. The error bars are only statistical. For the ψ', both the 1-D and 4-D deconvolution results are shown.

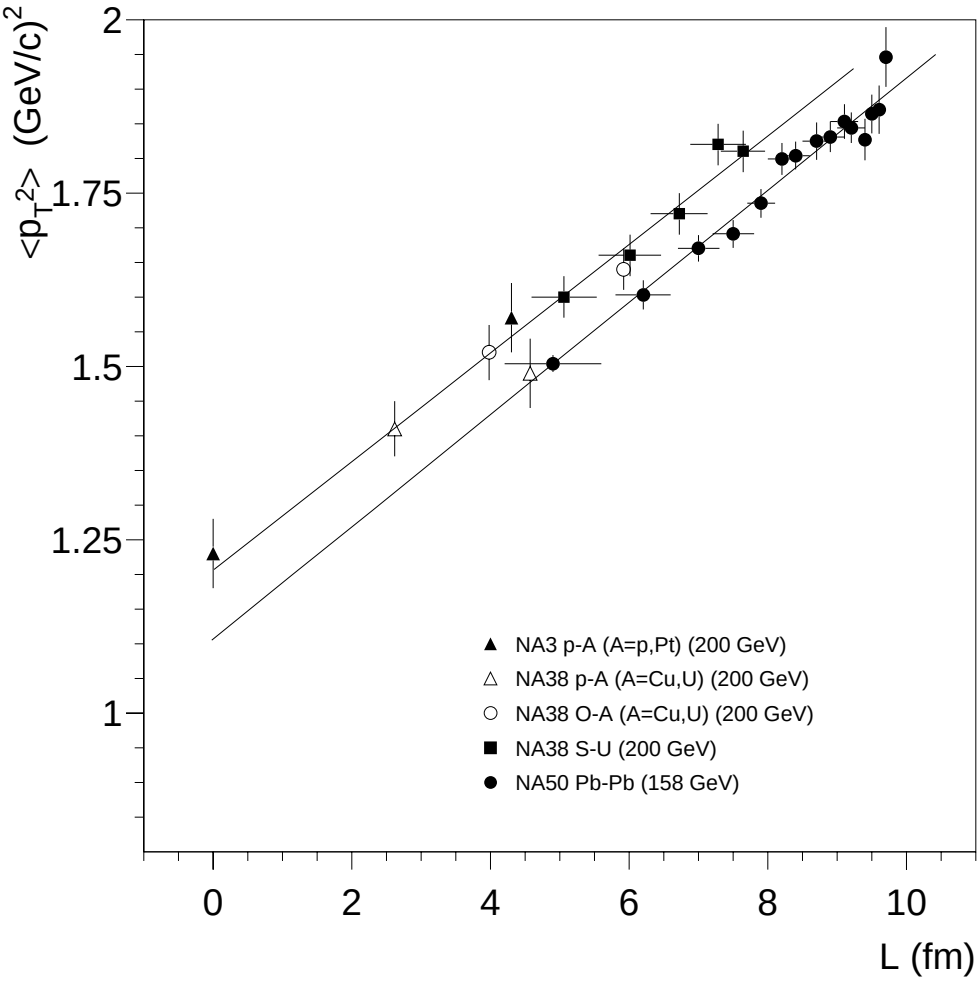

Figure 5: $\langle p_{\mathrm{T}}^2 \rangle$ values of the J/ψ as a function of L. The measurements performed at 200 GeV/nucleon are also included. The lines are linear fits to the data points, one for each beam energy.

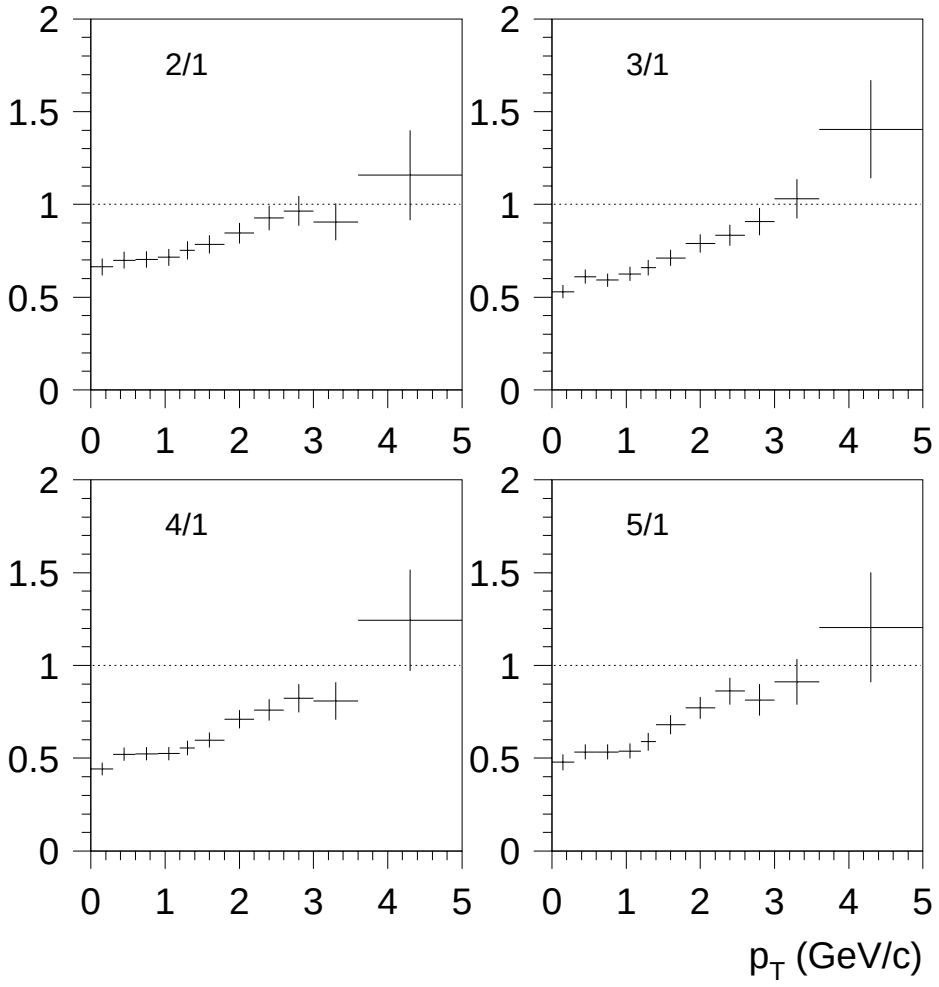

Figure 6: Ratios between the J/ψ $p_{\rm T}$ distributions in the $E_{\rm T}$ bin i ($i = 2, 3, 4, 5$) and in the first $E_{\rm T}$ bin, $R_i(p_{\rm T})$.

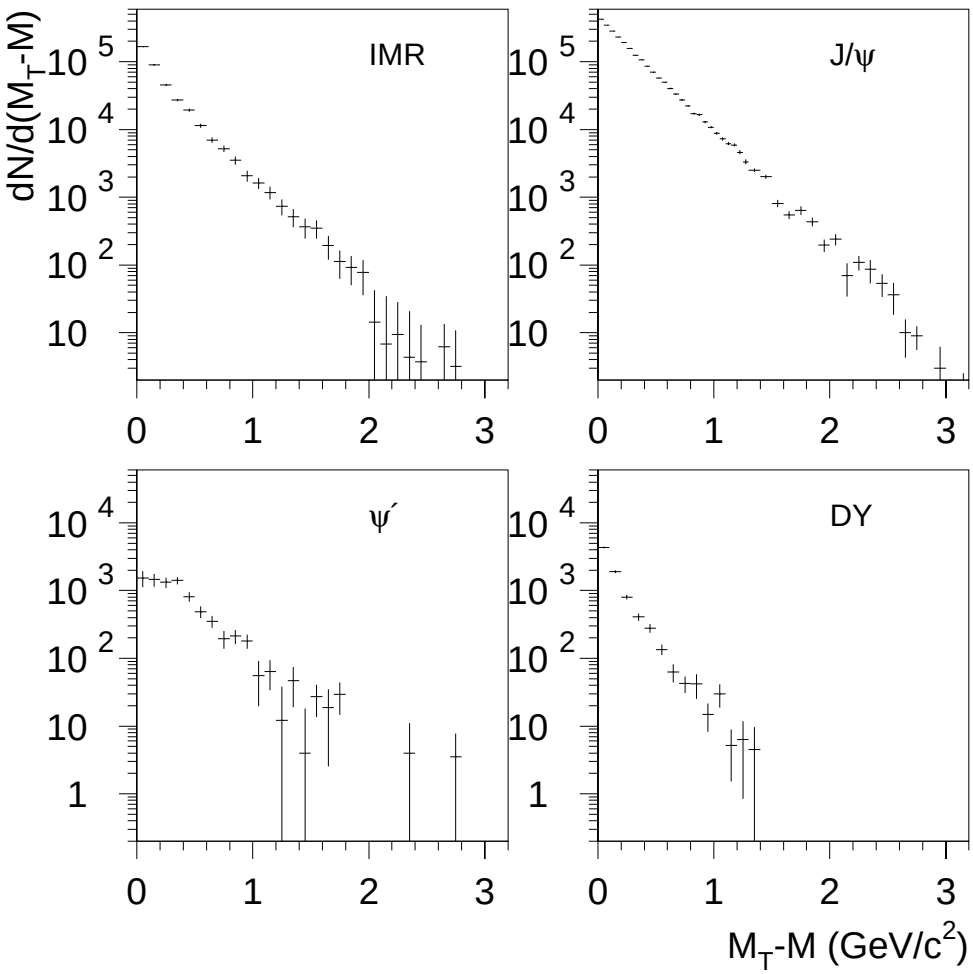

Figure 7: $M_{\mathrm{T}} - M$ distributions for several muon pair mass intervals.

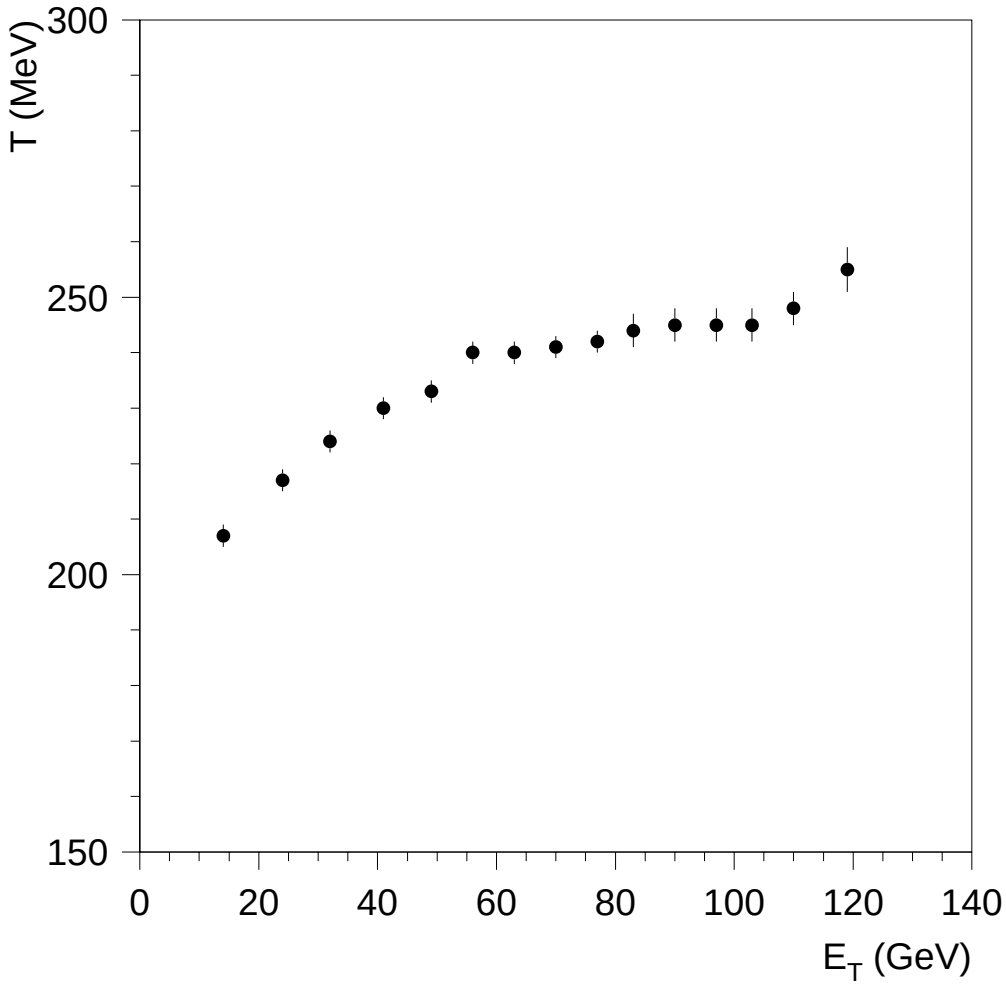

Figure 8: Inverse slope parameter, T, of the J/ψ transverse mass distributions, plotted as a function of the transverse energy.